HHS Public Access

Author manuscript

Neuroimage. Author manuscript; available in PMC 2021 February 01.

Published in final edited form as:

Neuroimage. 2020 February 01; 206: 116307. doi:10.1016/j.neuroimage.2019.116307.

Quantitative age-dependent differences in human brainstem myelination assessed using high-resolution magnetic resonance mapping

Mustapha Bouhrara[†,1], **Luis E. Cortina**[†,1], **Abinand C. Rejimon**[1], **Nikkita Khattar**[1], **Christopher Bergeron**[1], **Janet Bergeron**[1], **Denise Melvin**[2], **Linda Zukley**[2], **Richard G. Spencer**[1]

[1]Laboratory of Clinical Investigation, National Institute on Aging, National Institutes of Health, Baltimore, MD 21224, USA.

[2]Clinical Research Core, Office of the Scientific Director, National Institute on Aging, National Institutes of Health, Baltimore, MD 21225, USA

Abstract

Previous *in-vivo* magnetic resonance imaging (MRI)-based studies of age-related differences in the human brainstem have focused on volumetric morphometry. These investigations have provided pivotal insights into regional brainstem atrophy but have not addressed microstructural age-differences. However, growing evidence indicates the sensitivity of quantitative MRI to microstructural tissue changes in the brain. These studies have largely focused on the cerebrum, with very few MR investigations addressing age-dependent differences in the brainstem, in spite of its central role in the regulation of vital functions. Several studies indicate early brainstem alterations in a myriad of neurodegenerative diseases and dementias. The paucity of MR-focused investigations is likely due in part to the challenges imposed by the small structural scale of the brainstem itself as well as of substructures within, requiring accurate high-spatial resolution imaging studies. In this work, we applied our recently developed approach to high-resolution myelin water fraction (MWF) mapping, a proxy for myelin content, to investigate myelin differences with normal aging within the brainstem. In this cross-sectional investigation, we studied a large cohort (n = 125) of cognitively unimpaired participants spanning a wide age range (21-94 years) and found a decrease in myelination with age in most brainstem regions studied, while various regions exhibited a quadratic association between myelin and age. We believe that this study is the first investigation of MWF differences with normative aging in the adult brainstem. Further, our results provide reference MWF values.

Corresponding author: Mustapha Bouhrara, Ph.D. Laboratory of Clinical Investigations National Institute on Aging, National Institutes of Health, 251 Bayview Blvd, Baltimore MD, 21224. mustapha.bouhrara2@nih.gov. Phone Number: (+1) 4105588541.
[†]Equal contribution

Keywords

Brainstem; myelin water fraction; MRI; normal aging; BMC-mcDESPOT

1. INTRODUCTION

The human brain undergoes structural and macromolecular changes during normal aging which are often associated with neurocognitive and functional decline (1). As an important example, histopathological and magnetic resonance imaging (MRI) studies reveal marked degradation of the brain's white matter, including myelin loss, with aging (2-14). However, while this myelination trajectory has been well-documented in the cerebrum using various quantitative MRI techniques (7-10, 14-21), little work has been conducted to investigate age-differences in the myelin content of brainstem structures. In addition to functioning as a relay and integrative brain center, the brainstem plays an important role in motor function and pain sensation, alertness, and regulation of cardiac, respiratory, and vasomotor functions. Multiple studies suggest significant brainstem involvement in the early development of Alzheimer's and Parkinson's diseases with accompanying neuropsychiatric symptoms including disturbances in mood, emotion, appetite, and sleep, as well as confusion, agitation, and depression (22-26). Therefore, characterizing age-differences in brainstem microstructure could provide important insights into the functional, emotional, and motor alterations that accompany normative aging and neurodegeneration.

The small scale of brainstem structures renders MR-based studies particularly challenging. In fact, the average brainstem volume is about 34 cm^3; this in contrast to the cerebrum, with an average volume > 800 cm^3 (27). The average diameter of cross-sectional area of the major brainstem subdivisions is only ~18 mm for the midbrain, ~30 mm for the pons, and ~14 mm for the medulla. Therefore, it is evident that imaging at high-spatial resolution is critical to minimize partial volume effects between gray and white matter as well as between different substructures. In recent groundbreaking work (28), Lambert and colleagues reported a linear relationship between various conventional quantitative MRI measures, including apparent transverse and longitudinal relaxation rates (R_2*, R_1), and magnetization transfer saturation (MTS, (29)), and age in the brainstem (28). It was further found that certain gray matter brainstem substructures exhibited decreased MTS and relaxation rates or increased proton density in old subjects. These results were interpreted as indicators of axonal loss, demyelination, or increased iron accumulation in these specific gray matter regions. These conventional quantitative MRI measures are sensitive to myelin content, with the work of Lambert and colleagues therefore providing critical insights into microstructural differences with aging and pathology. Importantly, these metrics also show correlation with histologic measures of myelin (30, 31). Nevertheless, interpretation can be problematic due to their sensitivity to other tissue properties as well (32-36). The development of advanced MR methods based on multicomponent relaxometry to map myelin water fraction (MWF) (37-39), a surrogate of myelin content, have resulted in MR studies with much greater specificity to myelin, although, similar to DTI, relaxation times, and MT, MWF determination is ultimately based on underlying modeling assumptions.

Unfortunately, conventional approaches to mapping MWF require lengthy and clinically unacceptable acquisition times for whole-brain coverage and are also very sensitive to noise and instable due to the small signal from the myelin water component, making them impractical for high-resolution imaging (40-45). To address these limitations, we previously developed the Bayesian Monte Carlo multicomponent driven equilibrium single pulse observation of T_1 and T_2 analysis (BMC-mcDESPOT) as an alternative approach to multicomponent relaxometry (46-48). This method provides whole brain high-resolution MWF maps with higher accuracy and precision than conventional methods (47, 48) and within a clinically acceptable imaging time, and has been used to provide quantitative evidence of myelin loss in mild cognitive impairment and dementia (49). In the present work, building on Lambert's *et al.* study (28), our main goal is to investigate age-differences in myelin in the brainstem using this stabilized approach to myelin quantification. Thus, we applied BMC-mcDESPOT to define differences in myelin content in the brainstem with normative aging on a large cohort of cognitively unimpaired participants ($n = 125$) spanning an extended and well-sampled age range between 21 and 94 years. Our main goals are to characterize the regional association of myelination with age in specific brainstem regions, to provide reference values for MWF in the adult brainstem, and to develop further insights into regional brainstem maturation and aging in a life-span sample of healthy adults. We believe this to be the first *in-vivo* study to investigate age-differences in MWF of human brainstem.

2. MATERIAL & METHODS

2.1. Subjects

Cognitively unimpaired subjects (57 women, 52.6 ± 20.3 years; 68 men, 56.5 ± 22.9 years) were recruited from the Baltimore Longitudinal Study of Aging (BLSA), an ongoing study of normative aging in adults (50, 51), and the Genetic and Epigenetic Signatures of Translational Aging Laboratory Testing (GESTALT) study, an ongoing epidemiological, observational and longitudinal study of adults. The BLSA is a longitudinal cohort study funded and conducted by the National Institute on Aging (NIA) Intramural Research Program (IRP). Established in 1958, the BLSA enrolls community-dwelling adults with no major chronic conditions or functional impairments. The GESTALT study is also a study of healthy volunteers, initiated in 2015, and funded and conducted by the NIA IRP. The goal of this study is to evaluate multiple biomarkers related to aging. Note that these studies do not differ in their population characteristics, so that combining subjects from them poses no difficulty. We note that the inclusion and exclusion criteria for these two studies are essentially identical. The cohort for our current study consisted of 125 subjects spanning the age range between 21 and 94 years (54.7 ± 21.7 years) after removal of six imaging datasets with technically limited scans, caused by, for example, excessive motion. Figure 1 provides a detailed distribution of the number of participants per sex and age-decade. Participants underwent a Mini Mental State Examination (MMSE) with a maximum score of 30 (ours sample of men = 28.5 ± 1.5; women = 29 ± 1.4). Age ($p > 0.1$) and MMSE ($p > 05$) were not statistically different between men and women. Experimental procedures were performed in compliance with our local Institutional Review Board, and all subjects provided written informed consent.

2.2. Magnetic resonance imaging

All experiments were performed on a 3T whole body Philips MRI system (Achieva, Best, The Netherlands) using the internal quadrature body coil for transmission and an eight-channel phased-array head coil for reception. For each participant, a whole brain MWF map was derived using the BMC-mcDESPOT method (46-49). This protocol consists of ten 3D spoiled gradient recalled echo (SPGR) images acquired with flip angles of [2 4 6 8 10 12 14 16 18 20]°, echo time of 1.37 ms and repetition time of 5 ms, and ten 3D balanced steady state free precession (bSSFP) images acquired with flip angles of [2 7 11 16 24 32 40 60]°, echo time of 2.8 ms and repetition time of 5.8 ms; the TE value is slightly lower than TR/2 to ensure a complete spin refocusing (52). The bSSFP images were acquired with radiofrequency excitation pulse phase increments of 0° or 180° to account for off-resonance effects (47, 48, 53). All SPGR and bSSFP images were acquired with a voxel size of 1.6 mm × 1.6 mm × 1.6 mm. Further, we used the double-angle method (DAM) to correct for radiofrequency excitation inhomogeneity (54). The DAM protocol consists of two fast spin-echo images acquired with flip angles of 45° and 90°, echo time of 102 ms, repetition time of 3000 ms, and acquisition voxel size of 2.6 mm × 2.6 mm × 4 mm. All images were obtained with a field of view of 240 mm × 208 mm × 150 mm and reconstructed on the scanner to a voxel size of 1 mm × 1 mm × 1 mm. We emphasize that all MRI studies and ancillary measurements were performed with the same MRI system, running the same pulse sequences, at the same facility, and directed by the same investigators for both BLSA and GESTALT participants.

2.3. Image processing

2.3.1 Myelin water fraction mapping and image registration—For each subject, the scalp, ventricles, and other nonparenchymal regions within the acquired images were eliminated with the FMRIB Library Software (FSL) using the SPGR images averaged over all flip angles as the input image (55). A whole-brain MWF map was then generated for the extracted parenchymal regions using the BMC-mcDESPOT analysis (46-48). Briefly, BMC-mcDESPOT assumes a two-component non-exchanging system consisting of short and long T_1 and T_2 components. The short component corresponds to the signal of water trapped within the myelin sheets while the long component corresponds to intra/extra-cellular water. Analysis was performed explicitly accounting for nonzero TE as incorporated into our TE-corrected-mcDESPOT signal model (46). BMC-mcDESPOT permits determination of MWF in each voxel through marginalization over nuisance parameters, which in this case are the relaxation times. High-dimensional numerical integration is needed to perform this marginalization; this computational difficulty was addressed using the Monte Carlo sampling. MWF maps were visually inspected for motion artifacts, and six data sets with evident artifacts were omitted from further analysis. Finally, the averaged SPGR image was nonlinearly registered to the MNI space (MNI152_T1_1mm) using the FSL registration tools *FLIRT* and *FNIRT* (55-57). The computed transformation matrix was then applied to the MWF map using the *applywarp* tool function from the registration processing toolbox in FSL (55).

2.3.2 Region of interest segmentation—Fourteen brainstem structures were chosen as regions of interest (ROIs) from the Johns Hopkins University (JHU) ICGM-DTI 81 atlas

(58, 59) and the Talairach structural atlas provided in FSL in order to cover all the ROIs for this investigation (Figure 2). Six white matter ROIs were derived from the JHU atlas; these were within the superior cerebellar peduncle, middle cerebellar peduncle, inferior cerebellar peduncle, corticospinal tract, lemniscus tract, and pontine tract. Four additional white matter ROIs were derived from the Talairach atlas corresponding to the midbrain, pons, medulla, and whole brainstem white matter, while three gray matter ROIs were derived from the same atlas corresponding to the substantia nigra, red nucleus, and subthalamic nucleus. All ROIs were eroded to reduce partial volume effects and imperfect image registration using a kernel box of 2 voxels × 2 voxels × 2 voxels with the FSL tool *fslmaths*. The ROIs were further superimposed on the Harvard-Oxford brainstem atlas in FSL and manually corrected as indicated to avoid anatomic overlap with nearby brain regions. For each ROI, the mean MWF value was calculated for each subject from the normalized space, as well as the mean and standard deviation (SD) MWF values averaged over participants for each age-interval described by Fig. 1. We note that the MWF map calculation, image registration, and ROI segmentation were performed blinded to any information pertaining to the participants' age, sex and cognitive status.

2.4. Statistical analysis

For each ROI, a linear regression model was evaluated with MWF as the dependent variable and with sex and age as the independent variables. The initial model incorporated an interaction between sex and age which was removed if not significant, with the resulting parsimonious model then evaluated without this nonsignificant interaction term. Further, it has been shown that the myelin association with aging generally follows an inverted U-shape in the cerebrum and cerebellum (7, 21). Therefore, for each ROI we also evaluated a model that incorporates a quadratic age term, that is, age^2. Here again, MWF was the dependent variable, with sex, age, and age^2 as the independent variables, and interaction terms were assessed as above. Of the several available methods, we simply used the F-test as implemented in MATLAB; incorporation (or not) of the interaction terms or the quadratic age term was based on the significance of the F statistic. In all cases, the threshold for statistical significance was taken as $p < 0.05$ after correction for multiple ROI comparisons using the false discovery rate (FDR) method (60, 61).

3. RESULTS

Figure 3 illustrates the differences in MWF across the adult lifespan represented as maps averaged over all experimental subjects within the indicated 10-year intervals, for four representative slices covering the main anatomical subdivisions of the brainstem. These MWF maps exhibit substantial tissue contrast between different brainstem substructures. Visual inspection shows that different regions exhibit different trends of MWF as a function of age with the superior brainstem regions, especially the midbrain, exhibiting greater MWF values in comparison to the inferior brainstem regions such as the medulla. All of these results indicate the sensitivity of BMC-mcDESPOT for detecting microstructural differences in myelin content in various brainstem regions as well as at different ages.

Figure 4 shows the MWF derived values from all participants as a function of their age for 14 white matter and gray matter regions. We note that all ROIs included a large number of voxels (Table 1). The plots indicate a decrease in MWF from young adulthood through old age. The main effect of age was significant in all brain regions evaluated except for the middle cerebellar peduncle ($p > 0.1$ before FDR correction) (Table 1). In addition, the most rapid declines in MWF with age were found in the midbrain, red nucleus, and subthalamic nucleus regions, which exhibited the greatest negative slopes, while the slowest declines in MWF with age were found in the middle cerebellar peduncle region. The slope of MWF versus age for each of the rapidly declining regions was statistically significantly different from that of the slowest declining region ($p < 0.01$; Z-test computed as the difference between the two slopes divided by the standard error of the difference between the slopes (62)). Furthermore, the highest MWF values were found in the cerebral peduncle, midbrain, and the red nucleus, while the lowest MWF values were found in the subthalamic nucleus, the lemniscus tract, the substantia nigra, and the medulla (Table 2), with the regions of highest MWF values significantly different from the regions of lowest MWF ($p < 0.01$).

Linear regression analysis showed that the effect of sex was significant ($p < 0.05$) or close to significant ($p < 0.1$) in only three brainstem regions, namely, the middle cerebellar peduncle ($F = 6$, $p = 0.006$), the cerebral peduncle ($F = 3{,}2$, $p = 0.075$), and the corticospinal tract ($F = 4.3$, $p = 0.04$); however, significance did not survive the FDR correction ($p > 0.1$ after FDR correction; Table 1). In these brain regions, women showed a trend of 7 to 9 % higher myelin content than men. The interaction term between age and sex was also significant in only five brain regions before FDR correction, and in no regions after correction: the superior cerebellar peduncle ($F = 7.1$, $p = 0.009$; $p > 0.05$ after FDR correction), the middle cerebellar peduncle ($F = 7.7$, $p = 0.006$; $p > 0.05$ after FDR correction), the corticospinal tract ($F = 5.7$, $p = 0.02$; $p > 0.1$ after FDR correction), the pons ($F = 4.7$, $p = 0.03$; $p > 0.1$ after FDR correction), and the substantia nigra ($F = 5.1$, $p = 0.023$; $p > 0.1$ after FDR correction). In these regions, women showed a trend to a more rapid decline of MWF with age as compared to men ($p > 0.05$ for comparison of slopes of linear regression of MWF on age).

Finally, in accordance with literature results in the cerebrum, we evaluated a quadratic age term, age^2, in the linear regression model (7). The statistical analysis indicated that the effect of this term was significant ($p < 0.05$) or close to significant ($p < 0.1$) in only six brainstem regions, namely, the superior cerebral peduncle ($F = 2.9$, $p = 0.09$), the whole white matter ($F = 3.3$, $p = 0.07$), the midbrain ($F = 13.5$, $p = 0.0003$), the red nucleus ($F = 3.7$, $p = 0.057$), the subthalamic nucleus ($F = 7.9$, $p = 0.006$), and the substantia nigra ($F = 5.5$, $p = 0.021$). We note that, except the midbrain and the subthalamic nucleus, statistical significance did not survive the FDR correction. The regression plots for these regions incorporating a quadratic age term are shown in Figure 5.

4. DISCUSSION

Multiple studies have shown that myelin degeneration is a cardinal feature of the biological process of aging as well as of various neurodegenerative diseases (2, 49, 63-71). Myelin provides axonal insulation, essential for proper saltatory conduction, as well as contributing

to axonal viability. Therefore, myelin damage or loss inhibits normal nerve impulse transmission, resulting in a variety of neurologic manifestations (2, 49, 64, 66, 67, 70, 72-78). Although several studies have investigated myelination patterns within the cerebrum and established potential mechanisms for demyelination, very little comparable work has been conducted on the brainstem, in spite of its potentially central role in aging and dementia. Indeed, this work was motivated by the emerging evidence of brainstem involvement in the early development of Alzheimer's disease and other neurodegenerative diseases (22-26). In this cross-sectional study, conducted on a large cohort of cognitively unimpaired subjects, we showed that the brainstem exhibits myelination differences throughout the human lifespan using a stabilized measure of MWF. Our results indicate that brainstem white matter and gray matter substructures exhibit different myelination trends with normal aging.

One of our particular interests was to investigate whether the myelination pattern in the brainstem followed a progression similar to that observed in the cerebrum, that is, a progressive increase in myelination from young adulthood through middle age, followed by decrease through older age (7, 21). Therefore, in all cases, we evaluated the statistical significance of quadratic terms in the age-dependence of myelination. We found that this quadratic term was significant or close to statistical significance in six of the fourteen brainstem regions studied, with only a marginal trend seen in other regions. It is unclear whether this lack of a clear quadratic trend reflects the power of the present study given the effect size, or rather reflects the true biologic time course of myelination in the brainstem. We note that in fact, the brainstem is one of the earliest structures to demonstrate significant myelination, with significant myelin present even at the pre-term stage of development (79). In any event, in this dataset, any quadratic trend is substantially less pronounced than is observed in the cerebrum (7, 21). This likely reflects the structural and functional differences between the brainstem and the cerebrum. Indeed, the brainstem is primarily focused on integrating information for survival, proprioception, motion, and sensation, while the cerebrum integrates more complicated reactions to stimuli and processes information necessary for higher level functions such as perception, thought, learning, and memory. Therefore, it is plausible that the myelination patterns between these functionally and developmentally different regions of the brain would be different. However, it must also be recognized that the relative importance of the linear versus quadratic age trends in our model, and the specific values of the parameters and their significance, will exhibit some variability as a function of sampling density within age groups, range of ages incorporated, and consistency of data (80). In addition, the choice of a linear regression model is consistent with our visual inspection but may not describe the underlying biology. Thus, this choice must be regarded as an expedient to model the data rather than a description of underlying physiologic processes. Other models, such as piecewise linear, may serve equally well as data descriptors. Finally, our dataset is cross-sectional, so that the linear or quadratic age-associations of MWF observed here require further validation through longitudinal studies. Such work, motivated by the present results, is underway.

We observed a more rapid decrease of myelin in the deep gray matter regions of the brainstem including the red nucleus and the subthalamic nucleus as compared to most other regions evaluated; this is in agreement with Lambert *et al.* (28). Studies have shown that

these regions are particularly susceptible to increased iron deposition during the processes of normative aging and neurodegeneration (81-84). This iron may serve to catalyze free radical reactions promoting lipid peroxidation and oxidative tissue damage, promoting myelin breakdown and consequent additional release of iron (85). Moreover, the midbrain also exhibited a rapid decline of MWF with age. Consistent with this, morphometry-based studies have shown that the midbrain specifically exhibits significant atrophy with aging, in contrast to other brainstem regions (28, 86). Accelerated demyelination of the midbrain observed here, and subsequent axonal loss could explain these consistent observations. Further, we observed progressively decreasing myelin content from the superior to inferior brainstem. We speculate that this is because the midbrain, the most superior of the main brainstem structures, contains large bundles of myelinated axons, such as the cerebral peduncle, while the medulla, in the inferior position, contains cell bodies of most of the cranial nerves in addition to gray matter nuclei with unmyelinated axons. Finally, our results exhibit relatively large MWF values in the deep gray matter regions, especially in the red-nucleus and the substantia nigra. This could be due to a bias in MWF values resulting from increased iron. Indeed, it has been shown that diffusion of iron into the extracellular space may shorten the corresponding transverse relaxation time leading to an artificial overestimation of MWF values (87). Further *ex-vivo* or histological experiments are required to unambiguously elucidate the origin of this observation.

The effect of sex on myelination trajectory was significant in three brainstem regions, with women exhibiting overall a rapid decrease in MWF with age as compared to men, but these observations were not statistically significant after FDR correction. It is likely that our model is underpowered to detect such sex differences; therefore, an increased cohort size could provide further insights into differences in myelination between males and females. Indeed, sexual dimorphism in myelination would be consistent with the known differences in proliferation of oligodendrocytes and myelin proteins (88-90) which are modulated by sex steroids (91). Moreover, several studies, including MRI investigations, have revealed gender differences in brain maturational processes and emphasize the importance of myelination in understanding the mechanism of neuropsychiatric disorders (92-95). However, the literature remains sparse and further advanced investigations are required (96, 97). Nonetheless, because the brainstem is critical for basic brain functions and is a locus for many phylogenetically conserved functions and anatomy throughout mammals, sex dimorphism is not expected to be as pronounced in comparison to other higher-level cortical areas (98).

To our knowledge, only one quantitative *in-vivo* MRI study has been conducted to date that investigates regional microstructural age-differences in the adult human brainstem (28). Indeed, based on relaxation rates, proton density, and MTS, Lambert and colleagues have shown that different gray matter brainstem substructures exhibited decreased MTS or relaxation rates and increased proton density; as indicators of axonal loss, demyelination, and increased iron accumulation (28). Building on Lambert's *et al.* original study, our goal was to investigate age-differences in myelin content of the brainstem using our MWF method and to provide complementary insights regarding brainstem myelination with normative aging. While sensitive to tissue changes, conventional quantitative MRI methods are not specific to any particular microstructural process. For example, it is most often assumed that relaxation within each imaging voxel may be described by a single relaxation

component, although this assumption does not capture the structural and compositional complexity of brain tissue. In fact, a number of previous studies have demonstrated the presence of multicomponent relaxation processes in brain as a signature of compartmentation (37, 41, 47, 77, 99, 100). However, conventional single-component MRI approaches provide higher precision in derived parameter estimates as compared to multicomponent parameter estimates, while requiring greatly reduced acquisition time. This permits, as in Lambert's *et al.* study (28), investigation of multiple quantitative MRI parameters, in contrast to a single metric, providing complementary insights of the microstructural age-differences. The tradeoff for this is use of a model that is arguably less descriptive of tissue properties than is a multicompartment model. Nevertheless, our finding, overall, agrees with Lambert's *et al.* observation of decreasing myelin content with age in various brainstem substructures (28). However, as indicated by Lambert *et al.*, axonal loss may also occur with normal aging. It is unclear whether such axonal damage results from long-term demyelination and consequent lack of trophic support or is concurrent with it. Further investigations using multimodal approaches would provide further insights (28, 35). In fact, various metrics for myelin all have their important roles. MWF (*via* mcDESPOT or multiexponential T_2 or T_2* decay) provides a value that is in principle proportional to myelin content. MWF measures however do not provide any information regarding organizational structure, and may even incorporate fractionated and ineffective myelin fragments. DTI, on the other hand, is an excellent metric for architecture, providing insight into another crucial aspect of myelin health, even though the values are not proportional to myelin content. Magnetization transfer, similarly, provides insight into aspects of proximity and chemical communication between pools, as well as their mobility. Similarly, the relaxation times T_1 and T_2 provide information complementary, but not redundant with, these metrics.

Although multicomponent analysis accounting for compartmentation improves both sensitivity and specificity for myelin content (77, 99, 100), the conventional techniques for this analysis are very sensitive to noise and instable due to the small signal from the myelin water component (40, 41); this renders high-resolution imaging challenging, especially in the clinical setting. This issue is further exacerbated for brainstem MR imaging due to its small structure and complex anatomy; this could explain the lack of MR-based work investigating the myelination patterns of the brainstem with aging or pathology. In the present work, we used BMC-mcDESPOT method we have developed for MWF imaging (46-48, 101); this technique is a substantial extension of the mcDESPOT analysis introduced by Deoni and colleagues (53,102). While the original mcDESPOT work permits fast imaging and has been extensively used to characterize brain maturation and various neurodegenerative diseases (2, 49, 67, 103-105), the nonlinear least-squares analysis employed can lead to substantial inaccuracies (47, 48, 101, 106-108). In contrast, our Bayesian implementation greatly improves the accuracy and precision of the analysis, permitting much more reliable high-spatial resolution imaging (47, 48). This capability was critical in our study to accurately delineate small brainstem substructures while avoiding partial volume bias. We further note that the greatly enhanced stability of MWF mapping with BMC-mcDESPOT would permit even higher spatial resolution studies to be performed

as well, opening the possibility of investigating the myelination patterns of very small substructures within the brainstem, at the expense however of increased acquisition time.

One of the main challenges of *in-vivo* brainstem studies is accurate segmentation of its substructures. This is mainly due to their small size, requiring high-spatial resolution imaging, as well as relatively poor contrast between various regions. In our study, we conducted a careful examination of all ROIs, but some partial volume bias could nevertheless remain in the calculated MWF values due to *e.g.* imperfect image registration. We note that the MWF maps provide excellent contrast between various regions, which guided us in our segmentation (Fig. 2). In fact, the MWF maps exhibit better delineation of different brainstem substructures as compared to weighted images, and could help in developing new, or refining existing, brainstem atlases. We further note that fully-automated brainstem segmentation pipelines are available providing superior spatial precision (28); however, these analyses rely on multiple parametric mapping protocols.

Our work has limitations. Our cohort, although relatively large and spanning a wide and well-sampled age range, does not include very young participants (< 20 years old); this limitation derives from the exclusion criteria of the BLSA and GESTALT studies; inclusion of younger participants may influence the shape of the MWF-age trends (80). We also note that optimal uniform sampling across all age intervals was not fully achieved in this convenience sample of participants in ongoing research protocols. In fact, the number of subjects included between 50-69 years is relatively lower as compared to the other age decades. This may also influence the overall interpretability of myelination during the process of aging, as discussed above. Nevertheless, the inclusion of a large number of participants between the extremes of age, and with fairly uniform age distribution, enabled us to explore nonlinear models as well as nonmonotonic models. Further, in contrast to Lambert's *et al.* study (28), our analysis was based on ROIs which led to a loss in spatial precision. As additional issue is that mcDESPOT in general, including BMC-mcDESPOT, provides relatively higher MWF values as compared to MSE-based methods (108). This discrepancy is likely due several physiological and experimental factors that are not modeled in either mcDESPOT- or MSE-based signal formalisms. This includes exchange between water pools; studies have shown that water exchange has non-negligible effect on MWF determination (109, 110). However, incorporation of water exchange in conventional mcDESPOT signal modeling leads to very instable determination of MWF (101, 106, 107). We are currently investigating the potential of BMC-mcDESPOT analysis to improve MWF determination when water exchange is incorporated. Other parameters that may bias MWF estimation are magnetization transfer between free water protons and macromolecules, iron content, T_1 effects resulting from short TRs (in MSE), off-resonance effects, J- coupling, spin locking, internal gradients, differential and signal attenuation due to water diffusion in underlying compartments. However, this limitation applies to all existing MWF mapping methods (41, 111-113). Therefore, our MWF values would best serve as reference values only for studies based on similar MWF approaches. Finally, our dataset is cross-sectional, so that the trends observed here require further validation through longitudinal studies. Such work, motivated by the present results, is underway.

5. CONCLUSIONS

We have demonstrated the feasibility of high-resolution myelin imaging in the brainstem. We found that myelin content decreases with normal aging throughout brainstem regions, with substantial regional variation, as expected. Our work also provides reference MWF values for the main substructures of the brainstem, providing a baseline for investigations of neurodegenerative diseases, such as Alzheimer's and Parkinson's diseases.

ACKNOWLEDGEMENT

We gratefully acknowledge the Intramural Research Program of the National Institute on Aging of the National Institutes of Health.

7. FUNDING SOURCES

This work was supported by the Intramural Research Program of the National Institute on Aging of the National Institutes of Health.

8. REFERENCES

1. Niccoli T, Partridge L. Ageing as a Risk Factor for Disease. Current Biology. 2012;22(17):R741–R52. [PubMed: 22975005]
2. Dean DC 3rd, Hurley SA, Kecskemeti SR, O'Grady JP, Canda C, Davenport-Sis NJ, et al. Association of Amyloid Pathology With Myelin Alteration in Preclinical Alzheimer Disease. JAMA Neurol. 2017;74(1):41–9. [PubMed: 27842175]
3. Bartzokis G, Lu PH, Tingus K, Mendez MF, Richard A, Peters DG, et al. Lifespan trajectory of myelin integrity and maximum motor speed. Neurobiology of aging. 2010;31(9):1554–62. [PubMed: 18926601]
4. Tang Y, Nyengaard JR, Pakkenberg B, Gundersen HJ. Age-induced white matter changes in the human brain: a stereological investigation. Neurobiology of aging. 1997;18(6):609–15. [PubMed: 9461058]
5. Peters A The effects of normal aging on myelin and nerve fibers: a review. Journal of neurocytology. 2002;31(8–9):581–93. [PubMed: 14501200]
6. Masoro EJ, Austad SN. Preface In: Masoro EJ, Austad SN, editors. Handbook of the Biology of Aging (Sixth Edition). Burlington: Academic Press; 2005 p. xvii–xviii.
7. Arshad M, Stanley JA, Raz N. Adult age differences in subcortical myelin content are consistent with protracted myelination and unrelated to diffusion tensor imaging indices. NeuroImage. 2016;143:26–39. [PubMed: 27561713]
8. Sullivan EV, Pfefferbaum A. Diffusion tensor imaging and aging. Neuroscience & Biobehavioral Reviews. 2006;30(6):749–61. [PubMed: 16887187]
9. Michielse S, Coupland N, Camicioli R, Carter R, Seres P, Sabino J, et al. Selective effects of aging on brain white matter microstructure: A diffusion tensor imaging tractography study. NeuroImage. 2010;52(4):1190–201. [PubMed: 20483378]
10. Rathee R, Rallabandi VPS, Roy PK. Age-Related Differences in White Matter Integrity in Healthy Human Brain: Evidence from Structural MRI and Diffusion Tensor Imaging. Magnetic resonance insights. 2016;9:9–20. [PubMed: 27279747]
11. Hasan KM, Kamali A, Iftikhar A, Kramer LA, Papanicolaou AC, Fletcher JM, et al. Diffusion tensor tractography quantification of the human corpus callosum fiber pathways across the lifespan. Brain Res. 2009;1249:91–100. [PubMed: 18996095]
12. Inano S, Takao H, Hayashi N, Abe O, Ohtomo K. Effects of age and gender on white matter integrity. AJNR American journal of neuroradiology. 2011;32(11):2103–9. [PubMed: 21998104]
13. Yeatman JD, Wandell BA, Mezer AA. Lifespan maturation and degeneration of human brain white matter. Nature communications. 2014;5:4932-.

14. Fjell AM, Engvig A, Tamnes CK, Grydeland H, Walhovd KB, Westlye LT, et al. Life-Span Changes of the Human Brain White Matter: Diffusion Tensor Imaging (DTI) and Volumetry. Cerebral Cortex. 2009;20(9):2055–68. [PubMed: 20032062]
15. Faizy TD, Kumar D, Broocks G, Thaler C, Flottmann F, Leischner H, et al. Age-Related Measurements of the Myelin Water Fraction derived from 3D multi-echo GRASE reflect Myelin Content of the Cerebral White Matter. Scientific Reports. 2018;8(1):14991. [PubMed: 30301904]
16. Brickman AM, Meier IB, Korgaonkar MS, Provenzano FA, Grieve SM, Siedlecki KL, et al. Testing the white matter retrogenesis hypothesis of cognitive aging. Neurobiology of aging. 2012;33(8): 1699–715. [PubMed: 21783280]
17. Callaghan MF, Freund P, Draganski B, Anderson E, Cappelletti M, Chowdhury R, et al. Widespread age-related differences in the human brain microstructure revealed by quantitative magnetic resonance imaging. Neurobiology of aging. 2014;35(8):1862–72. [PubMed: 24656835]
18. Lee SM, Choi YH, You SK, Lee WK, Kim WH, Kim HJ, et al. Age-Related Changes in Tissue Value Properties in Children: Simultaneous Quantification of Relaxation Times and Proton Density Using Synthetic Magnetic Resonance Imaging. Investigative radiology. 2018;53(4):236–45. [PubMed: 29504952]
19. van der Flier WM, van den Heuvel DM, Weverling-Rijnsburger AW, Bollen EL, Westendorp RG, van Buchem MA, et al. Magnetization transfer imaging in normal aging, mild cognitive impairment, and Alzheimer's disease. Annals of neurology. 2002;52(1):62–7. [PubMed: 12112048]
20. Westlye LT, Walhovd KB, Dale AM, Bjornerud A, Due-Tonnessen P, Engvig A,. et al.Life-span changes of the human brain white matter: diffusion tensor imaging (DTI) and volumetry. Cerebral cortex (New York, NY : 1991). 2010;20(9):2055–68.
21. Bouhrara M, Rejimon AC, Cortina LE, Khattar N, Bergeron CM, Ferrucci L, et al. Adult brain aging investigated using BMC-mcDESPOT based myelin water fraction imaging. Neurobiology of aging. 2019; 10.1016/j.neurobiolaging.2019.10.003.
22. Simic G, Stanić G, Mladinov M, Jovanov-Milosevic N, Kostovic I, Hof PR. Annotation - Does Alzheimer's disease begin in the brainstem? Neuropathology and applied neurobiology. 2009;35(6):532–54. [PubMed: 19682326]
23. Lee JH, Ryan J, Andreescu C, Aizenstein H, Lim HK. Brainstem morphological changes in Alzheimer’s disease. Neuroreport. 2015;26(7):411–5. [PubMed: 25830491]
24. Grinberg LT, Rueb U, Heinsen H. Brainstem: Neglected Locus in Neurodegenerative Diseases. Frontiers in Neurology. 2011;2:42. [PubMed: 21808630]
25. Montplaisir J, Petit D, Lorrain D, Gauthier S, Nielsen T. Sleep in Alzheimer's disease: further considerations on the role of brainstem and forebrain cholinergic populations in sleep-wake mechanisms. Sleep. 1995;18(3):145–8. [PubMed: 7610309]
26. Rub U, Del Tredici K, Schultz C, Thal DR, Braak E, Braak H. The autonomic higher order processing nuclei of the lower brain stem are among the early targets of the Alzheimer's disease-related cytoskeletal pathology. Acta Neuropathol. 2001;101(6):555–64. [PubMed: 11515783]
27. Henery CC, Mayhew TM. The cerebrum and cerebellum of the fixed human brain: efficient and unbiased estimates of volumes and cortical surface areas. J Anat. 1989;167:167–80. [PubMed: 2630531]
28. Lambert C, Chowdhury R, Fitzgerald THB, Fleming SM, Lutti A, Hutton C, et al. Characterizing aging in the human brainstem using quantitative multimodal MRI analysis. Frontiers in human neuroscience. 2013;7:462-. [PubMed: 23970860]
29. Helms G, Dathe H, Kallenberg K, Dechent P. High-resolution maps of magnetization transfer with inherent correction for RF inhomogeneity and T1 relaxation obtained from 3D FLASH MRI. Magnetic resonance in medicine. 2008;60(6):1396–407. [PubMed: 19025906]
30. Schmierer K, Tozer DJ, Scaravilli F, Altmann DR, Barker GJ, Tofts PS, et al. Quantitative magnetization transfer imaging in postmortem multiple sclerosis brain. Journal of magnetic resonance imaging : JMRI. 2007;26(1):41–51. [PubMed: 17659567]
31. Schmierer K, Scaravilli F, Altmann DR, Barker GJ, Miller DH. Magnetization transfer ratio and myelin in postmortem multiple sclerosis brain. Annals of neurology. 2004;56(3):407–15. [PubMed: 15349868]

32. Alexander AL, Lee JE, Lazar M, Field AS. Diffusion tensor imaging of the brain. Neurotherapeutics : the journal of the American Society for Experimental NeuroTherapeutics. 2007;4(3):316–29. [PubMed: 17599699]
33. Deoni SC. Quantitative relaxometry of the brain. Topics in magnetic resonance imaging: TMRI. 2010;21(2):101–13. [PubMed: 21613875]
34. Winston GP. The physical and biological basis of quantitative parameters derived from diffusion MRI. Quantitative imaging in medicine and surgery. 2012;2(4):254–65. [PubMed: 23289085]
35. Uddin MN, Figley TD, Solar KG, Shatil AS, Figley CR. Comparisons between multi-component myelin water fraction, T1w/T2w ratio, and diffusion tensor imaging measures in healthy human brain structures. Scientific Reports. 2019;9(1):2500. [PubMed: 30792440]
36. Heath F, Hurley SA, Johansen-Berg H, Sampaio-Baptista C. Advances in noninvasive myelin imaging. Developmental neurobiology. 2018;78(2):136–51. [PubMed: 29082667]
37. MacKay A, Whittall K, Adler J, Li D, Paty D, Graeb D. In vivo visualization of myelin water in brain by magnetic resonance. Magnetic resonance in medicine. 1994;31(6):673–7. [PubMed: 8057820]
38. Prasloski T, Rauscher A, MacKay AL, Hodgson M, Vavasour IM, Laule C, et al. Rapid whole cerebrum myelin water imaging using a 3D GRASE sequence. NeuroImage. 2012;63(1):533–9. [PubMed: 22776448]
39. Whittall KP, MacKay AL, Graeb DA, Nugent RA, Li DK, Paty DW. In vivo measurement of T2 distributions and water contents in normal human brain. Magnetic resonance in medicine. 1997;37(1):34–43. [PubMed: 8978630]
40. Alonso-Ortiz E, Levesque IR, Pike GB. MRI-based myelin water imaging: A technical review. Magnetic resonance in medicine. 2015;73(1):70–81. [PubMed: 24604728]
41. Bouhrara M, Reiter DA, Maring MC, Bonny JM, Spencer RG. Use of the NESMA Filter to Improve Myelin Water Fraction Mapping with Brain MRI. Journal of neuroimaging. 2018;28(6): 640–649 [PubMed: 29999204]
42. Hwang D, Chung H, Nam Y, Du YP, Jang U. Robust mapping of the myelin water fraction in the presence of noise: synergic combination of anisotropic diffusion filter and spatially regularized nonnegative least squares algorithm. Journal of magnetic resonance imaging : JMRI. 2011;34(1): 189–95. [PubMed: 21618330]
43. Kumar D, Siemonsen S, Heesen C, Fiehler J, Sedlacik J. Noise robust spatially regularized myelin water fraction mapping with the intrinsic B1-error correction based on the linearized version of the extended phase graph model. Journal of magnetic resonance imaging : JMRI. 2016;43(4):800–17. [PubMed: 26477610]
44. Kwon OI, Woo EJ, Du YP, Hwang D. A tissue-relaxation-dependent neighboring method for robust mapping of the myelin water fraction. NeuroImage. 2013;74:12–21. [PubMed: 23384527]
45. Nam Y, Lee J, Hwang D, Kim DH. Improved estimation of myelin water fraction using complex model fitting. NeuroImage. 2015;116:214–21. [PubMed: 25858448]
46. Bouhrara M, Spencer RG. Incorporation of nonzero echo times in the SPGR and bSSFP signal models used in mcDESPOT. Magnetic resonance in medicine. 2015;74(5):1227–35. [PubMed: 26407635]
47. Bouhrara M, Spencer RG. Improved determination of the myelin water fraction in human brain using magnetic resonance imaging through Bayesian analysis of mcDESPOT. NeuroImage. 2016;127:456–71. [PubMed: 26499810]
48. Bouhrara M, Spencer RG. Rapid simultaneous high-resolution mapping of myelin water fraction and relaxation times in human brain using BMC-mcDESPOT. NeuroImage. 2017;147:800–11. [PubMed: 27729276]
49. Bouhrara M, Reiter D, Bergeron C, Zukley L, Ferrucci L, Resnick S, et al. Evidence of demyelination in mild cognitive impairment and dementia using a direct and specific magnetic resonance imaging measure of myelin content. Alzheimer's & Dementia. 2018;14(8):998–1004.
50. Ferrucci L The Baltimore Longitudinal Study of Aging (BLSA): a 50-year-long journey and plans for the future. The journals of gerontology Series A, Biological sciences and medical sciences. 2008;63(12):1416–9.

51. Shock N Normal Human Aging: The Baltimore Longitudinal Study of Aging. Journal of Gerontology. 1985;40(6):767-.
52. Scheffler K, Hennig J. Is TrueFISP a gradient-echo or a spin-echo sequence? Magnetic resonance in medicine. 2003;49(2):395–7. [PubMed: 12541263]
53. Deoni SC. Correction of main and transmit magnetic field (B0 and B1) inhomogeneity effects in multicomponent-driven equilibrium single-pulse observation of T1 and T2. Magnetic resonance in medicine. 2011;65(4):1021–35. [PubMed: 21413066]
54. Stollberger R, Wach P. Imaging of the active B1 field in vivo. Magnetic resonance in medicine. 1996;35(2):246–51. [PubMed: 8622590]
55. Jenkinson M, Beckmann CF, Behrens TE, Woolrich MW, Smith SM. FSL. NeuroImage. 2012;62(2):782–90. [PubMed: 21979382]
56. Jenkinson M, Smith S. A global optimisation method for robust affine registration of brain images. Medical image analysis. 2001;5(2):143–56. [PubMed: 11516708]
57. Jenkinson M, Bannister P, Brady M, Smith S. Improved optimization for the robust and accurate linear registration and motion correction of brain images. NeuroImage. 2002;17(2):825–41. [PubMed: 12377157]
58. Wakana S, Jiang H, Nagae-Poetscher LM, van Zijl PC, Mori S. Fiber tract-based atlas of human white matter anatomy. Radiology. 2004;230(1):77–87. [PubMed: 14645885]
59. Oishi Kenichi, Faria Andreia V., Peter C M van Zijl, Mori S. MRI Atlas of Human White Matter2010
60. Benjamini Y Discovering the false discovery rate. Journal of the Royal Statistical Society Series B (Statistical Methodology). 2010;72(4):405–16.
61. Benjamini Y, Hochberg Y. Controlling the False Discovery Rate: A Practical and Powerful Approach to Multiple Testing. Journal of the Royal Statistical Society Series B (Methodological). 1995;57(1):289–300.
62. PATERNOSTER R, BRAME R, MAZEROLLE P, PIQUERO A. USING THE CORRECT STATISTICAL TEST FOR THE EQUALITY OF REGRESSION COEFFICIENTS. Criminology. 1998;36(4):859–66.
63. Borich MR, MacKay AL, Vavasour IM, Rauscher A, Boyd LA. Evaluation of white matter myelin water fraction in chronic stroke. NeuroImage: Clinical. 2013;2:569–80. [PubMed: 24179808]
64. Flynn SW, Lang DJ, Mackay AL, Goghari V, Vavasour IM, Whittall KP, et al. Abnormalities of myelination in schizophrenia detected in vivo with MRI, and post-mortem with analysis of oligodendrocyte proteins. Molecular psychiatry. 2003;8(9):811–20. [PubMed: 12931208]
65. Laule C, Vavasour IM, Moore GR, Oger J, Li DK, Paty DW, et al. Water content and myelin water fraction in multiple sclerosis. A T2 relaxation study. Journal of neurology. 2004;251(3):284–93. [PubMed: 15015007]
66. Sirrs SM, Laule C, Madler B, Brief EE, Tahir SA, Bishop C, et al. Normal-appearing white matter in patients with phenylketonuria: water content, myelin water fraction, and metabolite concentrations. Radiology. 2007;242(1):236–43. [PubMed: 17185670]
67. Dean DC III, Sojkova J, Hurley S, Kecskemeti S, Okonkwo O, Bendlin BB, et al. Alterations of Myelin Content in Parkinson's Disease: A Cross-Sectional Neuroimaging Study. PloS one. 2016;11(10):e0163774. [PubMed: 27706215]
68. Faizy TD, Thaler C, Kumar D, Sedlacik J, Broocks G, Grosser M, et al. Heterogeneity of Multiple Sclerosis Lesions in Multislice Myelin Water Imaging. PloS one. 2016;11(3):e0151496. [PubMed: 26990645]
69. Manogaran P, Vavasour IM, Lange AP, Zhao Y, McMullen K, Rauscher A, et al. Quantifying visual pathway axonal and myelin loss in multiple sclerosis and neuromyelitis optica. NeuroImage: Clinical. 2016;11:743–50. [PubMed: 27330974]
70. Vargas WS, Monohan E, Pandya S, Raj A, Vartanian T, Nguyen TD, et al. Measuring longitudinal myelin water fraction in new multiple sclerosis lesions. NeuroImage Clinical. 2015;9:369–75. [PubMed: 26594620]
71. Bartzokis G Alzheimer's disease as homeostatic responses to age-related myelin breakdown. Neurobiology of aging. 2011;32(8):1341–71. [PubMed: 19775776]

72. Bartzokis G Age-related myelin breakdown: a developmental model of cognitive decline and Alzheimer's disease. Neurobiology of aging. 2004;25(1):5–18; author reply 49-62. [PubMed: 14675724]
73. Bartzokis G, Lu PH, Mintz J. Human brain myelination and amyloid beta deposition in Alzheimer's disease. Alzheimer's & dementia : the journal of the Alzheimer's Association. 2007;3(2):122–5.
74. Chamberlain KA, Nanescu SE, Psachoulia K, Huang JK. Oligodendrocyte regeneration: Its significance in myelin replacement and neuroprotection in multiple sclerosis. Neuropharmacology. 2016;110:633–43. [PubMed: 26474658]
75. Gold BT, Jiang Y, Powell DK, Smith CD. Multimodal imaging evidence for axonal and myelin deterioration in amnestic mild cognitive impairment. Journal of Alzheimer's disease : JAD. 2012;31 Suppl 3:S19–31. [PubMed: 22460327]
76. Kolind S, Matthews L, Johansen-Berg H, Leite MI, Williams SC, Deoni S, et al. Myelin water imaging reflects clinical variability in multiple sclerosis. NeuroImage. 2012;60(1):263–70. [PubMed: 22155325]
77. MacKay AL, Laule C. Magnetic Resonance of Myelin Water: An in vivo Marker for Myelin. Brain Plasticity. 2016;2(1):71–91. [PubMed: 29765849]
78. Nasrabady SE, Rizvi B, Goldman JE, Brickman AM. White matter changes in Alzheimer's disease: a focus on myelin and oligodendrocytes. Acta Neuropathologica Communications. 2018;6:22. [PubMed: 29499767]
79. van der Knaap MS, Valk J. MR imaging of the various stages of normal myelination during the first year of life. Neuroradiology. 1990;31(6):459–70. [PubMed: 2352626]
80. Fjell AM, Walhovd KB, Westlye LT, Ostby Y, Tamnes CK, Jernigan TL, et al. When does brain aging accelerate? Dangers of quadratic fits in cross-sectional studies. NeuroImage. 2010;50(4): 1376–83. [PubMed: 20109562]
81. Langkammer C, Ropele S, Pirpamer L, Fazekas F, Schmidt R. MRI for iron mapping in Alzheimer's disease. Neuro-degenerative diseases. 2014;13(2–3):189–91. [PubMed: 23942230]
82. Pfefferbaum A, Adalsteinsson E, Rohlfing T, Sullivan EV. MRI estimates of brain iron concentration in normal aging: comparison of field-dependent (FDRI) and phase (SWI) methods. NeuroImage. 2009;47(2):493–500. [PubMed: 19442747]
83. Wang D, Li W-B, Wei X-E, Li Y-H, Dai Y-M. An Investigation of Age-Related Iron Deposition Using Susceptibility Weighted Imaging. PloS one. 2012;7(11):e50706. [PubMed: 23226360]
84. Ward RJ, Zucca FA, Duyn JH, Crichton RR, Zecca L. The role of iron in brain ageing and neurodegenerative disorders. The Lancet Neurology. 2014;13(10):1045–60. [PubMed: 25231526]
85. Möller HE, Bossoni L, Connor JR, Crichton RR, Does MD, Ward RJ, et al. Iron, Myelin, and the Brain: Neuroimaging Meets Neurobiology. Trends in Neurosciences. 2019.
86. Luft AR, Skalej M, Schulz JB, Welte D, Kolb R, Burk K, et al. Patterns of age-related shrinkage in cerebellum and brainstem observed in vivo using three-dimensional MRI volumetry. Cerebral cortex (New York, NY : 1991). 1999;9(7):712–21.
87. Birkl C, Birkl-Toeglhofer AM, Endmayr V, Hoftberger R, Kasprian G, Krebs C, et al. The influence of brain iron on myelin water imaging. NeuroImage. 2019;199:545–52. [PubMed: 31108214]
88. Cerghet M, Skoff RP, Bessert D, Zhang Z, Mullins C, Ghandour MS. Proliferation and death of oligodendrocytes and myelin proteins are differentially regulated in male and female rodents. The Journal of neuroscience : the official journal of the Society for Neuroscience. 2006;26(5):1439–47. [PubMed: 16452667]
89. Yang S, Li C, Zhang W, Wang W, Tang Y. Sex differences in the white matter and myelinated nerve fibers of Long-Evans rats. Brain Research. 2008; 1216:16–23. [PubMed: 18486116]
90. Greer JM, Csurhes PA, Pender MP, McCombe PA. Effect of gender on T-cell proliferative responses to myelin proteolipid protein antigens in patients with multiple sclerosis and controls. Journal of Autoimmunity. 2004;22(4):345–52. [PubMed: 15120759]
91. Marin-Husstege M, Muggironi M, Raban D, Skoff RP, Casaccia-Bonnefil P. Oligodendrocyte Progenitor Proliferation and Maturation Is Differentially Regulated by Male and Female Sex Steroid Hormones. Developmental Neuroscience. 2004;26(2-4):245–54. [PubMed: 15711064]

92. De Bellis MD, Keshavan MS, Beers SR, Hall J, Frustaci K, Masalehdan A, et al. Sex Differences in Brain Maturation during Childhood and Adolescence. Cerebral Cortex. 2001;11(6):552–7. [PubMed: 11375916]

93. Menzler K, Belke M, Wehrmann E, Krakow K, Lengler U, Jansen A, et al. Men and women are different: diffusion tensor imaging reveals sexual dimorphism in the microstructure of the thalamus, corpus callosum and cingulum. NeuroImage. 2011;54(4):2557–62. [PubMed: 21087671]

94. Giedd JN, Raznahan A, Mills KL, Lenroot RK. Review: magnetic resonance imaging of male/female differences in human adolescent brain anatomy. Biology of sex differences. 2012;3(1):19-. [PubMed: 22908911]

95. Liu F, Vidarsson L, Winter JD, Tran H, Kassner A. Sex differences in the human corpus callosum microstructure: a combined T2 myelin-water and diffusion tensor magnetic resonance imaging study. Brain Res. 2010;1343:37–45. [PubMed: 20435024]

96. David SP, Naudet F, Laude J, Radua J, Fusar-Poli P, Chu I, et al. Potential Reporting Bias in Neuroimaging Studies of Sex Differences. Scientific Reports. 2018;8(1):6082. [PubMed: 29666377]

97. Jahanshad N, Thompson PM. Multimodal neuroimaging of male and female brain structure in health and disease across the life span. Journal of neuroscience research. 2017;95(1–2):371–9. [PubMed: 27870421]

98. Mashour GA, Alkire MT. Evolution of consciousness: phylogeny, ontogeny, and emergence from general anesthesia. Proc Natl Acad Sci U S A. 2013;110 Suppl 2:10357–64. [PubMed: 23754370]

99. Laule C, Kozlowski P, Leung E, Li DK, Mackay AL, Moore GR. Myelin water imaging of multiple sclerosis at 7 T: correlations with histopathology. NeuroImage. 2008;40(4):1575–80. [PubMed: 18321730]

100. Laule C, Leung E, Lis DK, Traboulsee AL, Paty DW, MacKay AL, et al. Myelin water imaging in multiple sclerosis: quantitative correlations with histopathology. Multiple sclerosis (Houndmills, Basingstoke, England). 2006;12(6):747–53.

101. Bouhrara M, Reiter DA, Celik H, Fishbein KW, Kijowski R, Spencer RG. Analysis of mcDESPOT- and CPMG-derived parameter estimates for two-component nonexchanging systems. Magnetic resonance in medicine. 2016;75(6):2406–20. [PubMed: 26140371]

102. Deoni SC, Rutt BK, Arun T, Pierpaoli C, Jones DK. Gleaning multicomponent T1 and T2 information from steady-state imaging data. Magnetic resonance in medicine. 2008;60(6):1372–87. [PubMed: 19025904]

103. Dean DC 3rd, O'Muircheartaigh J, Dirks H, Waskiewicz N, Lehman K, Walker L, et al. Estimating the age of healthy infants from quantitative myelin water fraction maps. Human brain mapping. 2015;36(4):1233–44. [PubMed: 25640476]

104. Deoni SC, Mercure E, Blasi A, Gasston D, Thomson A, Johnson M, et al. Mapping infant brain myelination with magnetic resonance imaging. The Journal of neuroscience : the official journal of the Society for Neuroscience. 2011;31(2):784–91. [PubMed: 21228187]

105. Deoni SC, Zinkstok JR, Daly E, Ecker C, Williams SC, Murphy DG. White-matter relaxation time and myelin water fraction differences in young adults with autism. Psychological medicine. 2015;45(4):795–805. [PubMed: 25111948]

106. West DJ, Teixeira RPAG, Wood TC, Hajnal JV, Tournier J-D, Malik SJ. Inherent and unpredictable bias in multi-component DESPOT myelin water fraction estimation. NeuroImage. 2019;195:78–88. [PubMed: 30930311]

107. Lankford CL, Does MD. On the inherent precision of mcDESPOT. Magnetic resonance in medicine. 2013;69(1):127–36. [PubMed: 22411784]

108. Zhang J, Kolind SH, Laule C, MacKay AL. Comparison of myelin water fraction from multiecho T2 decay curve and steady-state methods. Magnetic resonance in medicine. 2015;73(1):223–32. [PubMed: 24515972]

109. Harkins KD, Dula AN, Does MD. Effect of intercompartmental water exchange on the apparent myelin water fraction in multiexponential T2 measurements of rat spinal cord. Magnetic resonance in medicine. 2012;67(3):793–800. [PubMed: 21713984]

110. van Gelderen P, Duyn JH. White matter intercompartmental water exchange rates determined from detailed modeling of the myelin sheath. Magnetic resonance in medicine. 2019;81(1):628–38. [PubMed: 30230605]

111. Levesque IR, Chia CL, Pike GB. Reproducibility of in vivo magnetic resonance imaging-based measurement of myelin water. Journal of magnetic resonance imaging : JMRI. 2010;32(1):60–8. [PubMed: 20578011]

112. Myint W, Ishima R. Chemical exchange effects during refocusing pulses in constant-time CPMG relaxation dispersion experiments. Journal of biomolecular NMR. 2009;45(1–2):207–16. [PubMed: 19618276]

113. Majumdar S, Orphanoudakis SC, Gmitro A, O'Donnell M, Gore JC. Errors in the measurements of T2 using multiple-echo MRI techniques. II. Effects of static field inhomogeneity. Magnetic resonance in medicine. 1986;3(4):562–74. [PubMed: 3747818]

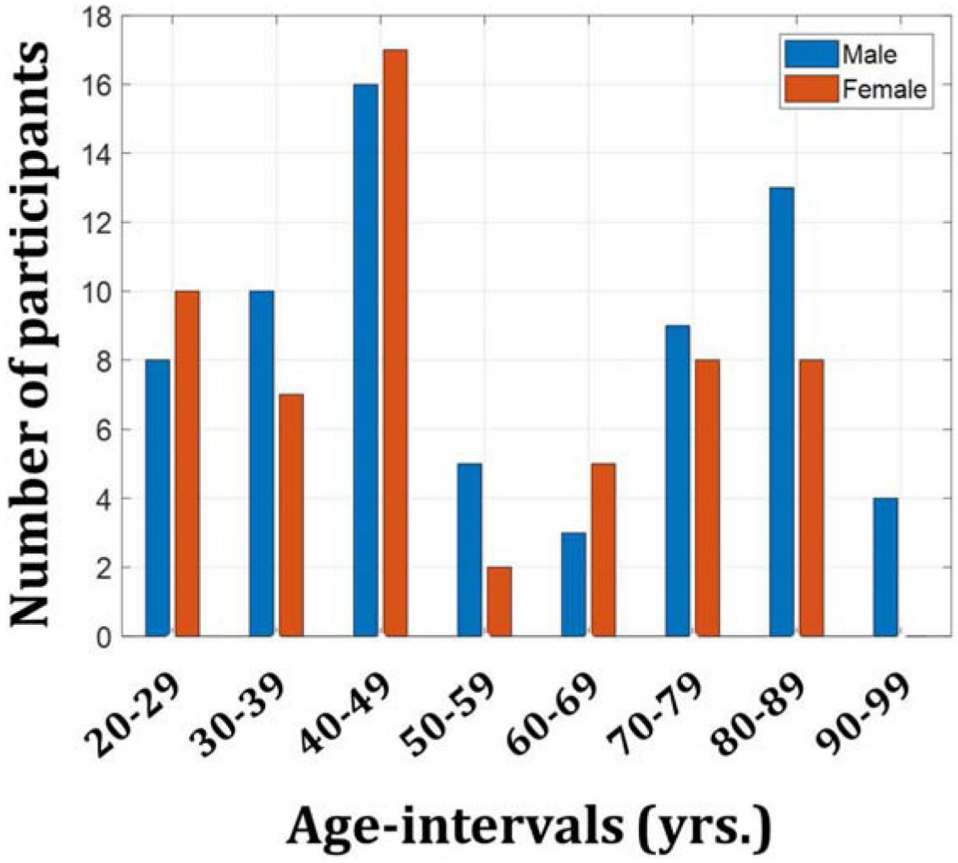

Figure 1. Number of participants per age-decade and sex within the study cohort.

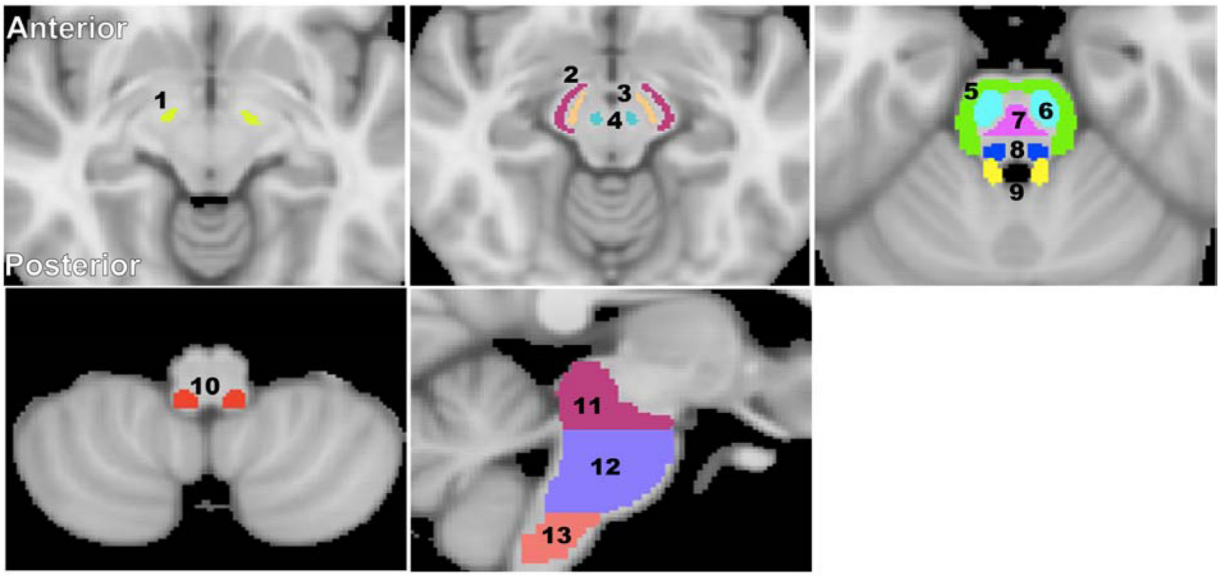

Figure 2: Visualization of the white matter and deep gray matter ROIs in the brainstem.
1) Subthalamic nucleus, 2) Cerebral peduncle, 3) Substantia nigra, 4) Red nucleus, 5) Middle cerebellar peduncle, 6) Corticospinal tract, 7) Pontine tract, 8) Lemniscus tract, 9) Superior cerebellar peduncle, 10) Inferior cerebellar peduncle, 11) Midbrain, 12) Pons, and 13) Medulla. The brain images were obtained from the standard MNI atlas provided in FSL.

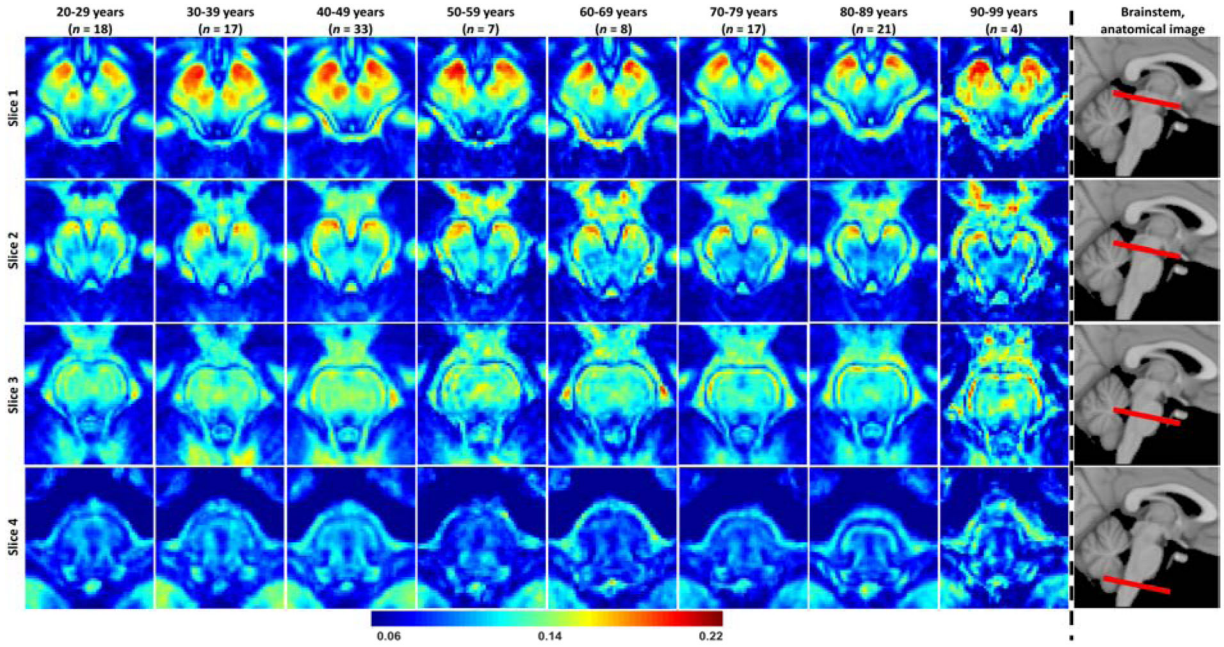

Figure 3: Myelin water fraction (MWF) represented as averaged participant maps calculated over 10-year intervals.

Results are shown for four representative slices covering the main brainstem structures. Slices 1 and 2 are representative axial views of the midbrain while slices 3 and 4 are representative axial views of the pons and medulla, respectively. The red bars on the anatomical images indicate the location of the slices. Visual inspection of MWF maps shows an increase in MWF values from early adulthood through middle age, that is, from 20-29 years through 40-49 years, followed by a more rapid decrease, in several brainstem substructures.

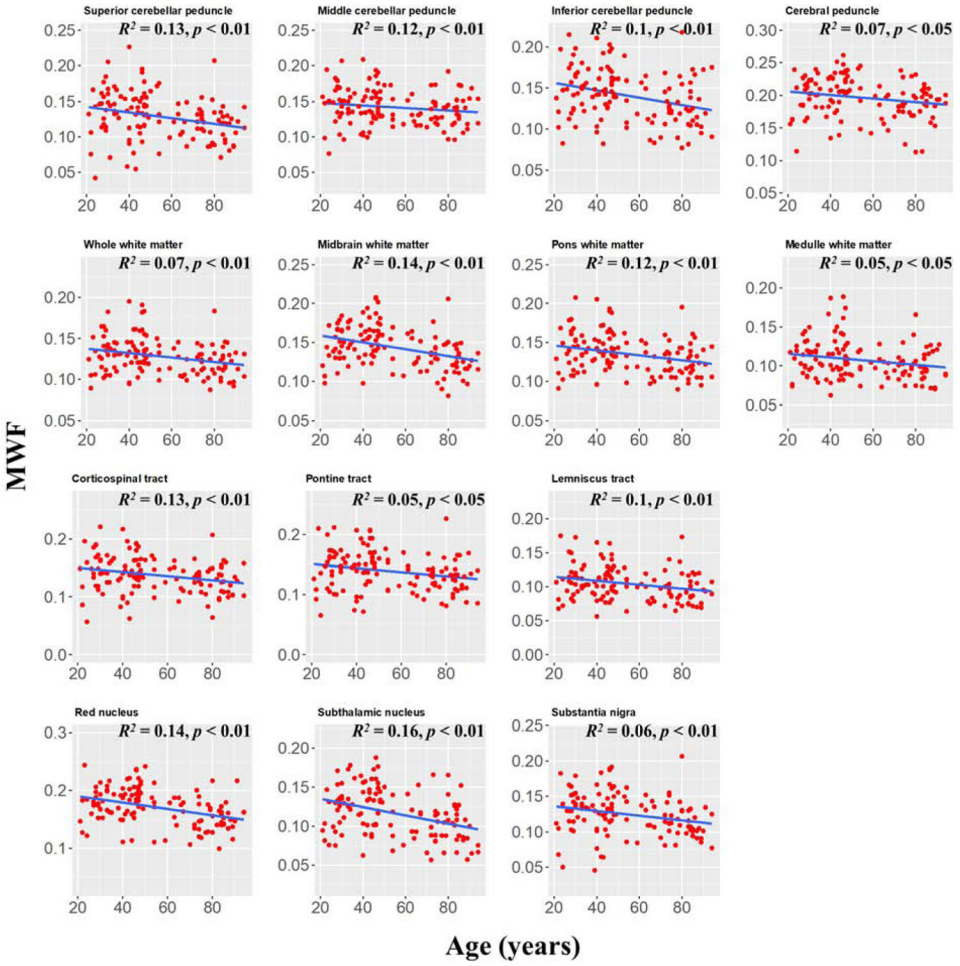

Figure 4: Plots of myelin water fraction (MWF) ROI values as a function of age (*N* = 125) for white and deep grey matter substructures within the brainstem.

For each region, the coefficient of determination, R^2, and the significance of the linear regression model, *p*, are reported. All regions investigated showed linearly decreasing trends of MWF with age while exhibiting variation in slope.

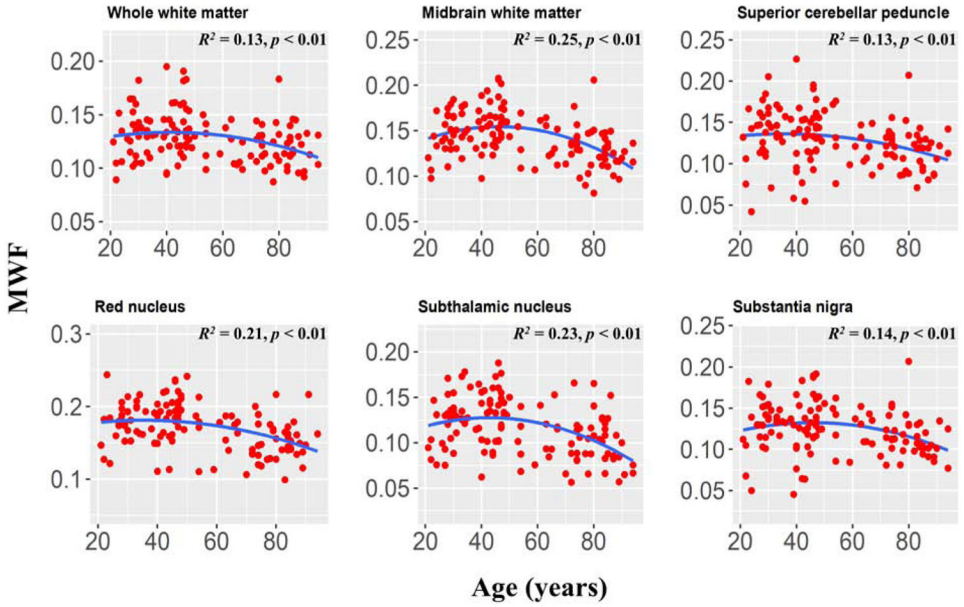

Figure 5: Plots of myelin water fraction (MWF) ROI values as a function of age (N = 125) for six of the substructures also highlighted in Fig. 4, but for which quadratic trends of MWF were significant.

For each region, the coefficient of determination, R^2, and the significance of the overall regression model, p, are reported. These selected regions clearly exhibited a quadratic trend of age on MWF, with significant or close to significant p values. This suggests progressive myelination continuing into middle age followed by more rapid myelin loss. We note that similar trends have recently been reported in the cerebrum (7, 21).

Table 1.

Significance of sex and age terms in the linear regressions. All p-values presented are obtained after FDR correction.

	Sex		Age	
	p	***F***	***p***	***F***
Superior cerebellar peduncle	0.48	0.9	0.006	9.4
Middle cerebellar peduncle	0.21	6.0	0.12	2.4
Inferior cerebellar peduncle	0.48	0.6	0.002	12.6
Cerebral peduncle	0.35	3.2	0.043	4.3
Corticospinal tract	0.28	4.3	0.009	7.5
Pontine tract	0.38	1.5	0.016	6.4
Lemniscus tract	0.48	0.8	0.008	8.3
Whole white matter	0.47	1.0	0.007	8.8
Midbrain white matter	0.37	1.7	0.0001	19.9
Pons white matter	0.36	2.0	0.006	9.4
Medulla white matter	0.73	0.1	0.02	5.6
Red nucleus	0.36	2.2	0.0001	19.9
Subthalamic nucleus	0.35	2.5	0.0001	20.0
Substantia nigra	0.46	0.6	0.009	7.7

Table 2.

The number of voxels in each ROI, and mean and standard deviation (SD) MWF values averaged over all participants for each ROI and for each age-interval as well as across the whole age-range.

	Mean ± SD MWF values									Number of voxels
	20-29 yrs.	30-39 yrs.	40-49 yrs.	50-59 yrs.	60-69 yrs.	70-79 yrs.	80-89 yrs.	90-99 yrs.	20-99 yrs.	
Superior cerebellar peduncle	0.131 ± 0.036	0.142 ± 0.035	0.136 ± 0.035	0.134 ± 0.039	0.121 ± 0.022	0.118 ± 0.021	0.115 ± 0.029	0.121 ± 0.016	0.128 ± 0.032	250
Middle cerebellar peduncle	0.147 ± 0.032	0.142 ± 0.025	0.147 ± 0.027	0.141 ± 0.025	0.133 ± 0.016	0.136 ± 0.019	0.136 ± 0.025	0.149 ± 0.021	0.142 ± 0.025	1934
Inferior cerebellar peduncle	0.147 ± 0.036	0.151 ± 0.023	0.153 ± 0.031	0.139 ± 0.032	0.122 ± 0.031	0.126 ± 0.022	0.128 ± 0.033	0.139 ± 0.041	0.140 ± 0.031	253
Cerebral peduncle	0.192 ± 0.033	0.206 ± 0.020	0.210 ± 0.030	0.200 ± 0.042	0.183 ± 0.025	0.187 ± 0.027	0.186 ± 0.031	0.194 ± 0.005	0.197 ± 0.030	2549
Corticospinal Tract	0.144 ± 0.038	0.145 ± 0.030	0.145 ± 0.033	0.141 ± 0.028	0.132 ± 0.024	0.128 ± 0.020	0.126 ± 0.031	0.130 ± 0.023	0.138 ± 0.031	1142
Pontine tract	0.140 ± 0.037	0.145 ± 0.033	0.152 ± 0.035	0.139 ± 0.029	0.128 ± 0.024	0.127 ± 0.022	0.128 ± 0.033	0.132 ± 0.035	0.139 ± 0.033	481
Lemniscus tract	0.109 ± 0.030	0.111 ± 0.020	0.112 ± 0.028	0.104 ± 0.021	0.094 ± 0.017	0.097 ± 0.021	0.097 ± 0.026	0.096 ± 0.008	0.105 ± 0.025	418
Whole white matter	0.129 ± 0.023	0.133 ± 0.018	0.138 ± 0.026	0.125 ± 0.018	0.118 ± 0.018	0.119 ± 0.016	0.121 ± 0.021	0.120 ± 0.014	0.128 ± 0.022	28977
Midbrain white matter	0.142 ± 0.024	0.155 ± 0.019	0.160 ± 0.025	0.140 ± 0.026	0.140 ± 0.020	0.131 ± 0.022	0.128 ± 0.025	0.125 ± 0.009	0.144 ± 0.026	8992
Pons white matter	0.137 ± 0.028	0.141 ± 0.022	0.146 ± 0.026	0.132 ± 0.022	0.123 ± 0.022	0.125 ± 0.019	0.127 ± 0.024	0.128 ± 0.018	0.135 ± 0.025	11577
Medulla white matter	0.109 ± 0.021	0.111 ± 0.023	0.116 ± 0.031	0.100 ± 0.016	0.099 ± 0.017	0.100 ± 0.016	0.099 ± 0.024	0.106 ± 0.021	0.107 ± 0.024	1838
Red nucleus	0.174 ± 0.029	0.183 ± 0.021	0.187 ± 0.030	0.174 ± 0.048	0.170 ± 0.017	0.148 ± 0.027	0.150 ± 0.024	0.172 ± 0.031	0.171 ± 0.031	646
Subthalamic nucleus	0.117 ± 0.027	0.135 ± 0.024	0.131 ± 0.029	0.106 ± 0.032	0.115 ± 0.024	0.097 ± 0.026	0.107 ± 0.028	0.077 ± 0.016	0.117 ± 0.030	280
Substantia nigra	0.125 ± 0.034	0.133 ± 0.027	0.132 ± 0.033	0.128 ± 0.033	0.128 ± 0.017	0.116 ± 0.022	0.113 ± 0.026	0.109 ± 0.026	0.125 ± 0.029	537